Research Square

Preprints are preliminary reports that have not undergone peer review.
They should not be considered conclusive, used to inform clinical practice,
or referenced by the media as validated information.

Pulsatile Red Reflex: Identification and Quantitative Characterization of a Previously Unreported Phenomenon

Abdulkadir Oduncu

abdulkadiroduncu@gmail.com

Liv Hospital Vadistanbul https://orcid.org/0000-0002-3370-8393

İbrahim Fırat Helvacıoğlu

Üsküdar University

Research Article

Keywords: pulsatile red reflex, red reflex, imaging photoplethysmography, ocular pulsatility, pulse rate, ophthalmic imaging

Posted Date: November 11th, 2026

DOI: https://doi.org/10.21203/rs.3.rs-11686540/v1

License: This work is licensed under a Creative Commons Attribution 4.0 International License.
Read Full License

Additional Declarations: The authors declare potential competing interests as follows: A.O. holds a financial interest in GlaucoT (Istanbul, Turkey), a medical technology company, and is an inventor on a pending patent application related to this work. I.F.H. declares no competing interests.

Abstract

Purpose

To describe and quantitatively characterize a previously unreported pulsatile component of the red reflex, which we term the pulsatile red reflex (PRR).

Methods

Thirty-one phakic participants underwent red-reflex video recording using a slit lamp and smartphone adapter after pharmacological mydriasis. A multichannel imaging photoplethysmography pipeline extracted pulse-related intensity changes. Relative signal amplitude and recording quality were characterized, and PRR-derived pulse rates were compared with contemporaneous fingertip pulse oximetry using Bland–Altman analysis.

Results

Twenty-one participants provided valid recordings (67.7%); three acquisitions failed because of dense posterior subcapsular cataract and seven did not meet the 10-s duration criterion. Green-channel root mean square alternating-to-direct-current (AC/DC) ratios ranged from 0.19% to 0.52% (median 0.28%). Reference pulse rates ranged from 55 to 90 beats per minute (bpm). Mean difference was + 0.03 bpm (SD 1.34), with 95% limits of agreement of − 2.60 to + 2.66 bpm. Mean absolute error was 1.04 bpm and root mean square error 1.31 bpm. Signed differences increased with the paired mean (slope 0.11 bpm/bpm; 95% confidence interval 0.07–0.15).

Conclusion

The familiar red reflex contains a measurable pulsatile intensity component at a frequency consistent with the peripheral pulse. These findings identify and quantitatively characterize PRR, with pulse rate agreement providing evidence of its pulse-related nature. PRR introduces a dynamic dimension to red-reflex assessment and a basis for further investigation of ocular pulsatile signals.

1 Introduction

The red reflex is a familiar clinical sign: light entering the eye is returned from the fundus through the pupil and appears as an orange-red glow under approximately coaxial illumination. For more than a century, its clinical interpretation has centred on colour, brightness, symmetry and media transparency, including its use in the Brückner test and paediatric screening [1, 2, 3, 4, 5]. Here, we describe a temporal property of this familiar sign: its intensity contains a measurable pulsatile component at a frequency consistent with the peripheral pulse. We term this phenomenon the pulsatile red reflex (PRR).

Ocular pulsatility and cardiac-cycle-dependent retinal reflectance changes have an established literature. Hassan and colleagues extracted pulse and respiration rates from vessel-resolved fundus images [6], and Tornow and colleagues mapped cardiac-cycle-induced attenuation changes in retinal tissue using video ophthalmoscopy [7]. Modified retinal photoplethysmography has also quantified vascular pulse amplitudes using slit-lamp ophthalmoscopy with a contact lens [8]. Separately, Choudhary and colleagues used multispectral images of the red-eye pupil reflection to assess oxygenation changes during normoxia and hypoxia [9]. These studies establish relevant optical and physiological foundations, but do not explicitly characterize the pulse-frequency intensity modulation of the clinical red reflex as the phenomenon described here.

The observation arose during routine slit-lamp work on iris-based imaging photoplethysmography (iPPG). Rather than resolving individual retinal vessels, we recorded the diffuse fundus glow visible within the pupil and examined its temporal intensity changes. PRR describes a property of the red reflex, not a particular instrument or extraction algorithm. Instruments that produce and permit recording of the red reflex, including ophthalmoscopes and surgical microscopes, are potential platforms for its investigation. The present study used slit-lamp video to document and quantify this property.

Our aim was to describe PRR and characterize its relative amplitude, recording yield and relationship to peripheral pulse rate. Camera-based iPPG methods provide tools for extracting small temporal intensity changes, including ambient-light measurements [10], chrominance-based extraction (CHROM) [11] and plane-orthogonal-to-skin (POS) projection [12]. Their performance depends on illumination, motion and processing [13, 14]. We adapted these approaches to red-reflex video and used agreement with fingertip pulse oximetry as quantitative evidence that the extracted oscillation was pulse-related. The study was designed as an initial characterization of the phenomenon and its measurement, without assigning a definitive anatomical source.

2 Methods

2.1 Study design and ethics

This single-centre observational study characterized a newly identified property of the red reflex and the feasibility of its video-based measurement at the outpatient ophthalmology clinic of Kağıthane Kızılay Hospital, Istanbul, Turkey. The study followed the Declaration of Helsinki and was approved by the Üsküdar University Non-Interventional Research Ethics Committee (2 June 2026, meeting no. 05; letter no. 61351342/020–152 dated 5 June 2026). Institutional permission was obtained. Written informed consent was obtained from participants; participants younger than 18 years provided assent together with consent from a parent or legal guardian.

2.2 Participants and recording protocol

Thirty-one phakic participants attending routine ophthalmic assessment were enrolled. Participants requiring dilation for their clinical examination were invited for red-reflex recording. Dilation used

tropicamide 1% and phenylephrine 2.5%. The target was an analysable recording of at least 10 s while the participant maintained fixation and minimised blinking. Recording duration and the presence of a usable red reflex determined acquisition success; software confidence flags were considered separately from this duration requirement.

Twenty-one participants provided a valid recording and a paired PRR–oximeter measurement for the agreement analysis. Three participants did not provide a usable red reflex because of dense posterior subcapsular cataract, and seven did not provide a recording meeting the 10-s duration criterion because of blinking or loss of fixation. Included participants were 13 female and 8 male, aged 16–65 years (mean 45.2 ± 13.5 years). Intraocular pressure measured by Goldmann applanation tonometry ranged from 12 to 21 mmHg (mean 16.1 ± 2.1 mmHg). Participant and recording characteristics are summarised in Table 1.

Table 1
Participant characteristics and recording parameters

Characteristic	**Value**
Participants enrolled	31
Participants with a valid paired recording	21
Acquisition failures	10 (3 media opacity; 7 duration < 10 s)
Recording yield, % (95% CI)	67.7 (50.1–81.4)
Sex, female/male, n	13/8
Age, years, mean ± SD	45.2 ± 13.5
Age, years, median (IQR)	46 (40–55)
Age range, years	16–65
IOP, mmHg, mean ± SD	16.1 ± 2.1
IOP, mmHg, median (IQR)	16 (15–17)
IOP range, mmHg	12–21
Lens status	Phakic
Mydriasis	Tropicamide 1% and phenylephrine 2.5%
Reference pulse rate range, bpm	55–90
Analysed recording duration range, s	10.3–22.3
Acquisition frame rate, frames/s	60
Minimum study recording duration, s	10

Demographic, IOP and rate summaries describe the 21 participants with valid recordings. CI, confidence interval; IOP, intraocular pressure; IQR, interquartile range; SD, standard deviation.

2.3 Equipment and reference measurement

Videos were acquired with a Haag-Streit BQ 900 slit lamp (Haag-Streit AG, Köniz, Switzerland) and an Apple iPhone 15 Pro mounted through a smartphone adapter. Blackmagic Camera software was used for ProRes 422 HQ recording at 3840 × 2160 pixels and 60 frames per second. Exposure and focus were locked, the illumination aperture was open, and the participant's head was supported by the slit-lamp chin and forehead rests. Analysis was performed offline.

A finger pulse oximeter (Contec CMS50D, Contec Medical Systems, Qinhuangdao, China) supplied the contemporaneous reference pulse rate. One displayed reference value was recorded for each included participant. Display resolution was 1 bpm. No electrocardiogram or synchronized reference plethysmographic waveform was acquired; the comparison therefore concerns pulse frequency rather than beat-by-beat phase or waveform morphology.

2.4 Signal processing

Processing was implemented in Python using PRR-Analyzer v47, NumPy and SciPy. The pipeline was developed iteratively on the recordings analysed in this report. CHROM and POS channels adapted published projections [11, 12] to ocular red, green and blue (RGB) traces. The processing sequence was intended to isolate and quantify the temporal component of the red reflex; its performance was evaluated in this development cohort.

Videos were decoded to RGB frames and resized to 320 pixels in width while preserving aspect ratio. An elliptical region of interest (ROI) covered the red-reflex region. The interface permits manual ROI placement and automatic initialisation from the brightest region of the spatially smoothed green channel. Frame-to-frame tracking used normalised cross-correlation (NCC) of a 16 × 16-pixel green-channel template within a 14-pixel search radius. Bright reflection pixels were excluded using an adaptive green-channel threshold (0.82 times the ROI's 99th percentile, constrained to 180–225 on the 8-bit scale), followed by 7 × 7-pixel mask dilation. Remaining ROI pixels were averaged separately for R, G and B. Missing samples were interpolated, followed by a logarithmic transformation and linear detrending.

CHROM and POS projections were formed from these transformed traces. Motion regression used horizontal and vertical ROI displacement, their squared terms and their interaction. Four extraction channels were evaluated: CHROM, POS, second-order blind identification (SOBI) and the green channel with singular spectrum analysis (G + SSA). SOBI used eight temporal lags; component selection considered cardiac-band signal-to-noise ratio (SNR), spectral sharpness, agreement with the chrominance estimate and artefact penalties. SSA used an adaptive embedding window of approximately 1.2 s, constrained by record length, and reconstructed qualifying cardiac-band components among the first six singular components.

Pulse rate estimation was restricted to 0.75–2.5 Hz (45–150 bpm). Welch power spectra used a Hann window and 50% overlap. For recordings shorter than 15 s the full record defined the segment length; longer records used the greater of 8 s or half the record length, capped at the full record length. Burg

autoregressive estimation (order 16; 4096-point frequency grid) was additionally evaluated for recordings shorter than 20 s. A Burg estimate could replace its Welch counterpart when their difference was below 10 bpm and Burg SNR exceeded 70% of Welch SNR. Multiple signal classification (MUSIC) was computed from a Kalman-smoothed SOBI signal (process variance 0.01, measurement variance 0.1) for diagnostic display and did not enter the final consensus.

SNR was calculated as the ratio of spectral power around the estimated fundamental and its first harmonic to remaining power within the cardiac search band, adapting the band-energy approach in [11]. The peak-centred half-width was twice the frequency-bin spacing, with a minimum of 0.06 Hz and a maximum of 15% of the 1.75-Hz search bandwidth. Harmonic power was included only where it fell within the search band. This estimate-centred SNR describes spectral concentration; it is not a reference-waveform validation metric. The green-channel alternating-to-direct-current (AC/DC) amplitude ratio was defined as the root mean square (RMS) of its fourth-order, zero-phase Butterworth-filtered cardiac-band component divided by the mean untransformed intensity, expressed as a percentage. The normalised signal quality index (NSQI) was the ratio of residual to cardiac-band root mean square amplitude, calculated from the CHROM trace. NCC, displacement, reflection exclusion and NSQI provided additional recording quality descriptors.

Candidate-specific screening considered spectral quality, suspected harmonic or common RGB artefacts and the number of valid ROI pixels. The largest candidate group was identified using a ± 6-bpm neighbourhood around each candidate estimate; ties were resolved by summed SNR. For a group containing at least two channels, the final estimate was its weighted mean. Effective normalised weights were proportional to channel SNR, with a 0.3 multiplier for channels failing their channel-specific eligibility check. The implemented recording-level quality multiplier was common to all channels and therefore cancelled in this normalised average; it did not provide independent channel-specific weighting. When no multichannel group was available, the implementation could return a single-channel fallback, followed by confidence downgrading according to recording quality flags. These software confidence rules were not equivalent to the study's ≥ 10-s acquisition criterion. Oximeter pulse rate was not an input to this extraction and fusion chain.

2.5 Statistical analysis

Differences were defined as PRR-iPPG minus reference pulse rate. Bland–Altman analysis [15] provided mean difference, sample standard deviation (SD) and 95% limits of agreement (LoA; mean difference ± 1.96 SD). The 95% confidence interval (CI) of mean difference used Student's t distribution with n − 1 degrees of freedom. Approximate CIs for each LoA used the same t quantile and standard error $\sqrt{(3s^2/n)}$, where s is the SD of differences. Normality was assessed with the Shapiro–Wilk test. MAE and RMSE were calculated from all 21 valid paired measurements.

Rate-related bias was explored by Pearson correlation and linear regression of difference against the paired mean, reporting the regression slope and its 95% CI. A sensitivity analysis excluded the two lowest-rate recordings. Spearman correlations explored associations between AC/DC and SNR, duration

and SNR, and duration and absolute error. Recording yield and the post hoc proportion within 2 bpm of the reference were reported with Wilson 95% CIs. The 2-bpm threshold was descriptive. No formal sample size calculation was performed for this initial observational study. Analyses used Python and SciPy, with two-sided p values and an exploratory significance threshold of 0.05; multiple exploratory comparisons were not adjusted.

2.6 Use of artificial intelligence

Claude (Anthropic) and ChatGPT (OpenAI) assisted with manuscript drafting and language editing, review of the signal-processing description and recalculation of tabulated summary statistics. The authors reviewed and edited the resulting material and retain responsibility for the data, methods, interpretation and final manuscript.

3 Results

3.1 PRR amplitude and recording yield

A measurable pulse-related component was extracted from 21 of 31 participants (67.7%; Wilson 95% CI 50.1–81.4%). Three acquisitions failed because dense posterior subcapsular cataract prevented a usable red reflex, and seven were shorter than 10 s because of blinking or loss of fixation. The following amplitude, quality and pulse rate results describe the 21 valid recordings.

Valid recording durations ranged from 10.3 to 22.3 s. Table 2 gives all 21 paired measurements and their quality descriptors. Green-channel AC/DC ranged from 0.19% to 0.52% (mean 0.30 ± 0.09%; median 0.28%). SNR ranged from 1.39 to 8.86 (mean 4.60 ± 1.91); 13 of 21 recordings exceeded 4.0. NCC ranged from 0.61 to 1.00 (mean 0.86 ± 0.12; median 0.88).

Table 2
Participant level quality descriptors and paired pulse rate measurements

ID	Duration (s)	NCC	AC/DC (%)	PRR (bpm)	Reference (bpm)	Difference (bpm)	Absolute error (bpm)	SNR	IOP (mmHg)
1	20.1	1.00	0.30	68.7	70.0	-1.3	1.3	4.21	16
2	18.5	0.94	0.19	83.6	82.0	+ 1.6	1.6	8.86	17
3	21.4	0.98	0.24	82.5	82.0	+ 0.5	0.5	6.43	15
4	19.8	0.87	0.26	82.8	83.0	-0.2	0.2	5.17	16
5	22.3	0.91	0.21	78.6	79.0	-0.4	0.4	4.98	18
6	15.2	0.83	0.31	72.5	72.0	+ 0.5	0.5	3.76	14
7	16.8	0.86	0.28	73.4	73.0	+ 0.4	0.4	4.12	15
8	20.6	0.95	0.22	89.9	90.0	-0.1	0.1	7.33	17
9	21.0	0.97	0.20	89.4	88.0	+ 1.4	1.4	6.88	19
10	14.5	0.79	0.35	68.4	70.0	-1.6	1.6	2.81	14
11	13.8	0.74	0.33	68.9	70.0	-1.1	1.1	2.54	15
12	17.2	0.88	0.23	85.8	83.0	+ 2.8	2.8	5.62	20
13	18.9	0.86	0.25	82.5	81.0	+ 1.5	1.5	5.01	16
14	11.5	0.72	0.38	73.1	73.0	+ 0.1	0.1	3.44	15
15	11.2	0.68	0.41	70.0	70.0	+ 0.0	0.0	2.92	16
16	20.4	0.93	0.27	82.1	81.0	+ 1.1	1.1	5.38	17
17	10.3	0.64	0.52	52.6	55.0	-2.4	2.4	1.39	12
18	19.1	0.90	0.22	82.7	82.0	+ 0.7	0.7	6.11	15
19	10.8	0.61	0.48	52.5	55.0	-2.5	2.5	1.52	14
20	12.1	0.97	0.30	72.0	73.0	-1.0	1.0	3.28	16
21	16.7	1.00	0.33	83.6	83.0	+ 0.6	0.6	4.74	21

Difference = PRR-iPPG minus pulse oximetry. AC/DC is the root mean square cardiac-band green-channel amplitude relative to its mean intensity. SNR is reported on a linear scale as supplied for each recording. NCC, normalised cross-correlation; IOP, intraocular pressure. PRR-iPPG estimates and errors are reported to one decimal place.

AC/DC was negatively associated with SNR (Spearman r = −0.91, p < 0.001). Duration was positively associated with SNR (r = 0.82, p < 0.001), but not significantly associated with absolute error (r = −0.18, p = 0.43). These exploratory associations do not establish causation.

3.2 Pulse rate agreement

Reference pulse rate ranged from 55 to 90 bpm and PRR-iPPG estimates from 52.5 to 89.9 bpm. Mean difference was + 0.03 bpm (95% CI − 0.58 to + 0.64), with SD 1.34 bpm and 95% LoA of − 2.60 to + 2.66 bpm. Approximate 95% CIs were − 3.66 to − 1.54 bpm for the lower LoA and + 1.60 to + 3.72 bpm for the upper LoA. MAE was 1.04 bpm and RMSE 1.31 bpm (Table 3; Fig. 1). The Shapiro–Wilk statistic was 0.978 (p = 0.89).

Table 3
Agreement statistics for the 21 valid paired measurements

Statistic	Estimate
Mean difference, bpm (95% CI)	+ 0.03 (− 0.58 to + 0.64)
SD of differences, bpm	1.34
Lower 95% LoA, bpm (95% CI)	−2.60 (− 3.66 to − 1.54)
Upper 95% LoA, bpm (95% CI)	+ 2.66 (+ 1.60 to + 3.72)
MAE, bpm	1.04
RMSE, bpm	1.31
Within sample-derived 95% LoA, n/N (%)	20/21 (95.2)
Within 2 bpm, n/N (%; Wilson 95% CI)	18/21 (85.7; 65.4–95.0)
Difference–mean correlation, r (p)	0.80 (< 0.001)
Difference–mean slope, bpm/bpm (95% CI)	0.11 (0.07–0.15)
Correlation excluding the two lowest rates, r (p)	0.65 (0.003)
Reference pulse rate range, bpm	55–90
Paired mean range, bpm	53.8–90.0
Shapiro–Wilk W (p)	0.978 (0.89)

CIs for LoA are approximate t-based intervals using SE = √(3s²/n). The ± 2-bpm analysis is post hoc and descriptive. LoA, limits of agreement; MAE, mean absolute error; RMSE, root mean square error. Pooled LoA do not remove the observed rate-related bias.

Each point represents one valid participant-level measurement (n = 21). Differences are PRR-iPPG minus pulse oximetry. The solid red line denotes mean difference (+ 0.03 bpm); dashed blue lines denote 95% limits of agreement (− 2.60 to + 2.66 bpm). Pale bands around the limits show their approximate 95%

confidence intervals. The grey dotted line is the exploratory regression of difference on paired mean (slope 0.11 bpm/bpm). Participant 12 is outlined. The regression illustrates rate-related bias; it was not used to calibrate the reported estimates

Twenty of 21 measurements were within the sample-derived LoA. Participant 12 had a difference of + 2.8 bpm, just beyond the upper LoA. Eighteen of 21 valid recordings were within 2 bpm of the reference (85.7%; Wilson 95% CI 65.4–95.0%).

Signed differences increased with the paired mean (Pearson $r = 0.80$, $p < 0.001$). The regression slope was 0.11 bpm per bpm (95% CI 0.07–0.15), corresponding to approximately 1.1 bpm change in signed error per 10 bpm increase in paired mean. The two recordings with reference rate 55 bpm were underestimated by 2.4 and 2.5 bpm; they were also the shortest recordings and had the lowest SNR and NCC. After their exclusion, the association persisted ($r = 0.65$, $p = 0.003$). Thus, the low pooled mean difference coexisted with rate-related estimation bias, with pulse rate, duration and quality partly confounded.

4 Discussion

This study identifies and quantitatively characterizes PRR, a pulsatile intensity component of the familiar red reflex. In 21 valid recordings, the extracted frequency closely matched the peripheral pulse, with MAE 1.04 bpm and pooled LoA − 2.60 to + 2.66 bpm. Green-channel RMS AC/DC ratios of 0.19–0.52% provide a quantitative description of the recorded modulation. Together, these findings support a dynamic, pulse-related dimension of the red reflex that is not captured by its conventional assessment of colour, symmetry and transparency.

To our knowledge, PRR has not previously been explicitly described and quantitatively characterized as a property of the clinical red reflex. This claim is distinct from the established observation of pulsatile retinal reflectance. Prior retinal iPPG studies resolved vessels or retinal tissue [6, 7, 8], whereas red-eye pupil-reflection oximetry assessed spectral changes with oxygenation [9]. Our observation concerns temporal intensity modulation of the diffuse red reflex itself. The slit lamp provided the recording platform in this study; it does not define the phenomenon. Pulse rate estimation serves here as a quantitative link to peripheral pulsatility. The processing sequence and extraction components are summarized in Fig. 2 and Table 4, with selected prior work placed in context in Table 5.

Elliptical ROI tracking and reflection masking provide RGB traces for log transformation and detrending. Motion regression is applied after projection for CHROM/POS and before SOBI/SSA. Spectral pulse rate estimates undergo candidate screening, neighbourhood selection and SNR-based fusion, with single-channel fallbacks and recording-level quality flags. MUSIC is a diagnostic output rather than a consensus input. The oximeter reference is used only for subsequent agreement analysis. ROI, region of interest; NCC, normalised cross-correlation; PSD, power spectral density; AR, autoregressive

Table 4
Extraction and fusion components in PRR Analyzer v47

Component	Principle	Implementation
CHROM	Adapted chrominance projection [11]	Applied to logarithmically transformed, detrended ocular RGB traces; followed by motion regression.
POS	Adapted orthogonal projection [12]	Applied to the same transformed ocular RGB traces, followed by motion regression; candidate screening includes valid-pixel count.
SOBI	Second-order source separation	Eight temporal lags; selected component evaluated with spectral quality and agreement criteria. Direct component estimate enters fusion; Kalman-smoothed signal supports diagnostics.
G + SSA	Adaptive green-channel reconstruction	Window approximately 1.2 s, constrained by record length; qualifying components among the first six are reconstructed.
Spectral estimation	Welch; conditional Burg AR	45–150 bpm search; Burg order 16 for records < 20 s under the stated replacement rule. MUSIC is diagnostic and excluded from consensus.
Fusion and quality flags	Candidate neighbourhood and weighted mean	Largest group within ± 6 bpm of a candidate; SNR-based relative weights and eligibility penalties. Single-channel fallbacks and recording-level confidence downgrades are retained.

CHROM, chrominance-based method; POS, plane-orthogonal-to-skin; SOBI, second-order blind identification; SSA, singular spectrum analysis; AR, autoregressive. These adapted channels share the same video data and are not independent physiological measurements.

Table 5
Context of selected facial and ocular iPPG studies

Study	Signal and approach	Sample	Context
de Haan and Jeanne 2013 [11]	Facial skin; CHROM	117 participants	Foundational chrominance-based pulse extraction.
Wang et al. 2017 [12]	Facial skin; POS	60 video sequences□	Algorithmic model and benchmark across recording challenges.
Debnath and Kim 2025 [13]	Facial rPPG; review	Multiple datasets	Review-level context; not a single accuracy experiment.
Acharya et al. 2025 [14]	Facial rPPG; multiple methods	45 in CHILL cohort	Illumination and elevated-rate challenges; broader rate range than the present cohort.
Hassan et al. 2018 [6]	Vessel-resolved fundus iPPG	5 healthy participants	Fundus camera mounted on a slit lamp; distinct from diffuse red-reflex acquisition.
Tornow et al. 2018 [7]	Retinal tissue video plethysmography	Instrument and application examples	Spatially resolved cardiac-cycle-induced retinal attenuation.
Abdul-Rahman et al. 2020 [8]	Retinal vascular mPPG	28 eyes of 16 participants	Slit-lamp imaging through a contact lens; vascular pulse attenuation.
Choudhary et al. 2019 [9]	Multispectral red-eye pupil reflection	10 healthy participants	Oxygenation changes under normoxia and hypoxia; pulse-frequency modulation was not the reported outcome.
Present study	Diffuse fundus red reflex	31 enrolled; 21 valid	Initial characterization of PRR; RMS AC/DC 0.19–0.52%, MAE 1.04 bpm and pooled LoA − 2.60 to + 2.66 bpm; rate-related estimation bias.

□ Video sequences are not a count of unique participants; the benchmark's unique total is not specified. Studies differ in reference, duration, rate coverage, inclusion and failure handling; the table provides context rather than a head-to-head accuracy comparison.

The vascular choroid is a plausible contributor to PRR because of its substantial blood supply and pulsatile perfusion [16, 17, 18]. Light contributing to the red reflex interacts with fundus tissue on its inward and outward paths; this provides an optical basis for investigating modulation by blood volume and absorption [5, 9]. A double-pass enhancement is a hypothesis, because neither optical path length nor amplification was measured here. Choroidal autoregulation also makes a purely passive model incomplete [19]. The anatomical and optical contributors to PRR can be investigated separately from its initial description as a pulse-related intensity phenomenon.

Intensity modulation can arise from changes in absorption and scattering, as well as from pulse-related movement of the eye, pupil or head. Reflection masking, tracking and motion regression were used to reduce contamination, but spatial controls and synchronized physiological recordings would help separate these contributions. Such experiments should clarify which components of PRR reflect blood-volume changes and which reflect optical or mechanical coupling. The present pulse rate comparison establishes frequency correspondence, rather than a unique physiological mechanism.

Amplitude and signal quality were not interchangeable in this cohort. Higher RMS AC/DC ratios were associated with lower SNR, so a larger measured modulation did not necessarily represent a cleaner physiological signal. The estimate-centred SNR describes spectral concentration around the selected frequency. Amplitude comparisons with facial rPPG require matched definitions and preprocessing; no amplitude or accuracy advantage over facial methods is inferred here [11, 12, 13, 14, 20, 21].

PRR is conceptually accessible wherever the red reflex can be produced and recorded with suitable illumination and observation geometry. Surgical microscopes and ophthalmoscopes are therefore potential acquisition platforms, while the present measurements were obtained only with the stated slit-lamp configuration. Stable positioning and a dilated pupil may facilitate acquisition, making the surgical microscope a useful next platform to examine. The 67.7% recording yield identifies practical barriers in the present setup: media opacity and blinking or loss of fixation. Whether alternative platforms, natural pupils or different wavelengths improve access to PRR remains to be tested.

The main limitations concern the extent of characterization and the generalizability of the extraction performance. There were 21 valid recordings from one centre, over a pulse rate range of 55–90 bpm, and the same recordings supported algorithm development and evaluation. The integer-valued pulse oximeter reference permitted frequency comparison but not phase or morphology analysis. Rate-related estimation bias remained despite the near-zero pooled mean difference, and formal test–retest assessment was not performed. These limitations define the scope of this initial report; it does not evaluate diagnostic performance for ocular or systemic disease.

Further work should establish repeatability, evaluate other red-reflex acquisition platforms, and distinguish optical, vascular and mechanical contributions using synchronized reference waveforms and spatial controls. Independent cohorts with fixed extraction rules and broader pulse rate coverage can evaluate estimation performance. The broader scientific opportunity is to determine which physiological information is carried by the temporal behaviour of a clinical sign that is already readily accessible in ophthalmic examination.

5 Conclusion

The red reflex contains a measurable pulsatile intensity component at a frequency consistent with the peripheral pulse. We identify and quantitatively characterize this property as the pulsatile red reflex (PRR). In 21 valid recordings, PRR-derived pulse rates showed close agreement with fingertip pulse oximetry, supporting the pulse-related nature of the phenomenon. PRR adds a dynamic dimension to a long-

established clinical sign and provides a basis for further investigation of ocular pulsatility across red-reflex imaging platforms.

Declarations

Funding

No funding was received for this study.

Competing interests

A.O. holds a financial interest in GlaucoT (Istanbul, Turkey), a medical technology company, and is an inventor on a pending patent application related to this work. I.F.H. declares no competing interests.

Author contributions

A.O. conceived the study, developed the signal-processing pipeline, recorded the data, performed the analysis and drafted the manuscript. I.F.H. contributed to study design, ethics approval, interpretation of the results and critical revision. Both authors reviewed and approved the manuscript.

Ethics approval

Üsküdar University Non-Interventional Research Ethics Committee, 2 June 2026 (meeting no. 05), letter no. 61351342/020-152 dated 5 June 2026. Institutional permission was obtained. The study followed the Declaration of Helsinki.

Consent to participate

Written informed consent was obtained from participants; assent and parental or legal guardian consent were obtained for participants younger than 18 years.

Data availability

The participant-level numerical data supporting the agreement analysis are presented in Table 2. Raw videos are not publicly available because of participant privacy. Access to recordings may be considered by the corresponding author subject to consent and institutional requirements.

Code availability

The PRR-Analyzer v47 code is available from the corresponding author upon reasonable request.

Prior presentation

Preliminary results were included in ESCRS 2026 poster PP19.017 (London, September 2026) and were accepted for poster presentation at the 60th National Congress of the Turkish Ophthalmological Society (Antalya, 25–29 November 2026; PS-0744).

References

1. Brückner R (1962) Exakte Strabismusdiagnostik bei 1/2–3jährigen Kindern mit einem einfachen Verfahren, dem «Durchleuchtungstest». Ophthalmologica 144(3):184–198. https://doi.org/10.1159/000304320
2. Tongue AC, Cibis GW (1981) Brückner test. Ophthalmology 88(10):1041–1044. https://doi.org/10.1016/S0161-6420(81)80034-6
3. Nguyen M, Blair K (2023) Red reflex. In: StatPearls [Internet]. StatPearls Publishing, Treasure Island (FL). Updated 28 August 2023. https://www.ncbi.nlm.nih.gov/books/NBK553139/. Accessed 8 November 2026
4. Vempuluru VS (2025) The red reflex test: a simple tool to detect alarming pediatric eye disease. Indian J Clin Exp Ophthalmol 11(3):371–372. https://doi.org/10.18231/j.ijceo.v.11.i.3.2
5. Roe LD, Guyton DL (1984) The light that leaks: Brückner and the red reflex. Surv Ophthalmol 28(6):665–670. https://doi.org/10.1016/0039-6257(84)90187-5
6. Hassan H, Jaidka S, Dwyer VM, Hu S (2018) Assessing blood vessel perfusion and vital signs through retinal imaging photoplethysmography. Biomed Opt Express 9(5):2351–2364. https://doi.org/10.1364/BOE.9.002351
7. Tornow RP, Odstrcilik J, Kolar R (2018) Time-resolved quantitative inter-eye comparison of cardiac cycle-induced blood volume changes in the human retina. Biomed Opt Express 9(12):6237–6254. https://doi.org/10.1364/BOE.9.006237
8. Abdul-Rahman A, Morgan W, Yu DY (2020) Measurement of normal retinal vascular pulse wave attenuation using modified photoplethysmography. PLoS ONE 15(5):e0232523. https://doi.org/10.1371/journal.pone.0232523
9. Choudhary TR, Ball D, Fernandez Ramos J, Stefansson E, Harvey AR (2019) Remote sensing of blood oxygenation using red-eye pupil reflection. Physiol Meas 40(12):12NT01. https://doi.org/10.1088/1361-6579/ab5f3b
10. Verkruysse W, Svaasand LO, Nelson JS (2008) Remote plethysmographic imaging using ambient light. Opt Express 16(26):21434–21445. https://doi.org/10.1364/OE.16.021434
11. de Haan G, Jeanne V (2013) Robust pulse rate from chrominance-based rPPG. IEEE Trans Biomed Eng 60(10):2878–2886. https://doi.org/10.1109/TBME.2013.2266196

12. Wang W, den Brinker AC, Stuijk S, de Haan G (2017) Algorithmic principles of remote-PPG. IEEE Trans Biomed Eng 64(7):1479–1491. https://doi.org/10.1109/TBME.2016.2609282
13. Debnath U, Kim S (2025) A comprehensive review of heart rate measurement using remote photoplethysmography and deep learning. Biomed Eng Online 24:73. https://doi.org/10.1186/s12938-025-01405-5
14. Acharya B, Saakyan W, Hammer B, Drimalla H (2025) The reliability of remote photoplethysmography under low illumination and elevated heart rates. NPJ Digit Med 8:744. https://doi.org/10.1038/s41746-025-02192-y
15. Bland JM, Altman DG (1986) Statistical methods for assessing agreement between two methods of clinical measurement. Lancet 1(8476):307–310. https://doi.org/10.1016/S0140-6736(86)90837-8
16. Nickla DL, Wallman J (2010) The multifunctional choroid. Prog Retin Eye Res 29(2):144–168. https://doi.org/10.1016/j.preteyeres.2009.12.002
17. Sugiyama T, Araie M, Riva CE, Schmetterer L, Orgul S (2010) Use of laser speckle flowgraphy in ocular blood flow research. Acta Ophthalmol 88(7):723–729. https://doi.org/10.1111/j.1755-3768.2009.01586.x
18. Sugiyama T (2014) Basic technology and clinical applications of the updated model of laser speckle flowgraphy to ocular diseases. Photonics 1(3):220–234. https://doi.org/10.3390/photonics1030220
19. Riva CE, Titze P, Hero M, Petrig BL (1997) Effect of acute decreases of perfusion pressure on choroidal blood flow in humans. Invest Ophthalmol Vis Sci 38(9):1752–1760. https://pubmed.ncbi.nlm.nih.gov/9286263/
20. Stricker R, Müller S, Gross HM (2014) Non-contact video-based pulse rate measurement on a mobile service robot. In: The 23rd IEEE International Symposium on Robot and Human Interactive Communication, Edinburgh, UK, pp 1056–1062. https://doi.org/10.1109/ROMAN.2014.6926392
21. Bobbia S, Macwan R, Benezeth Y, Mansouri A, Dubois J (2019) Unsupervised skin tissue segmentation for remote photoplethysmography. Pattern Recognit Lett 124:82–90. https://doi.org/10.1016/j.patrec.2017.10.017

Figures

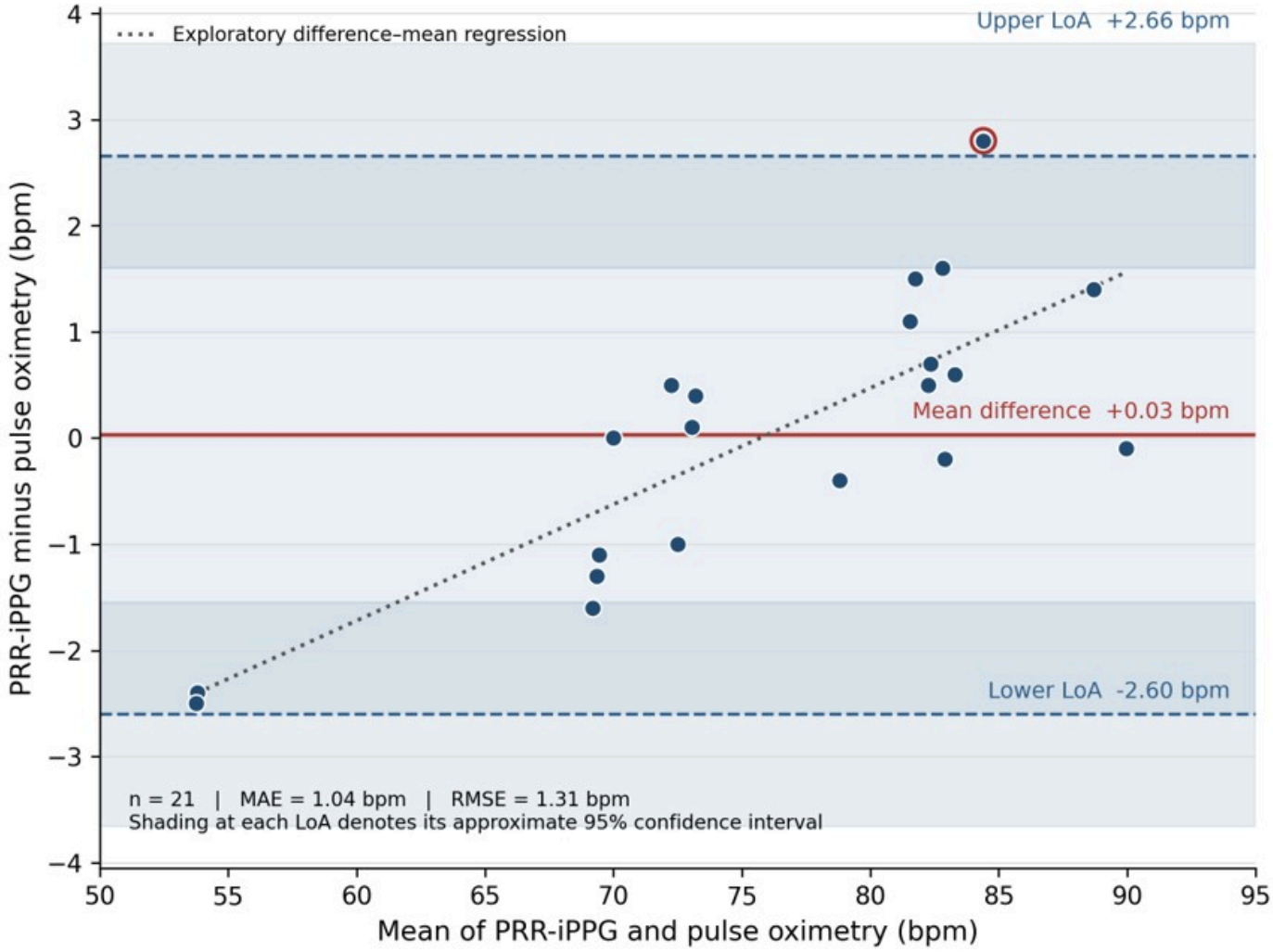


Figure 1

Agreement between PRR iPPG and pulse oximetry

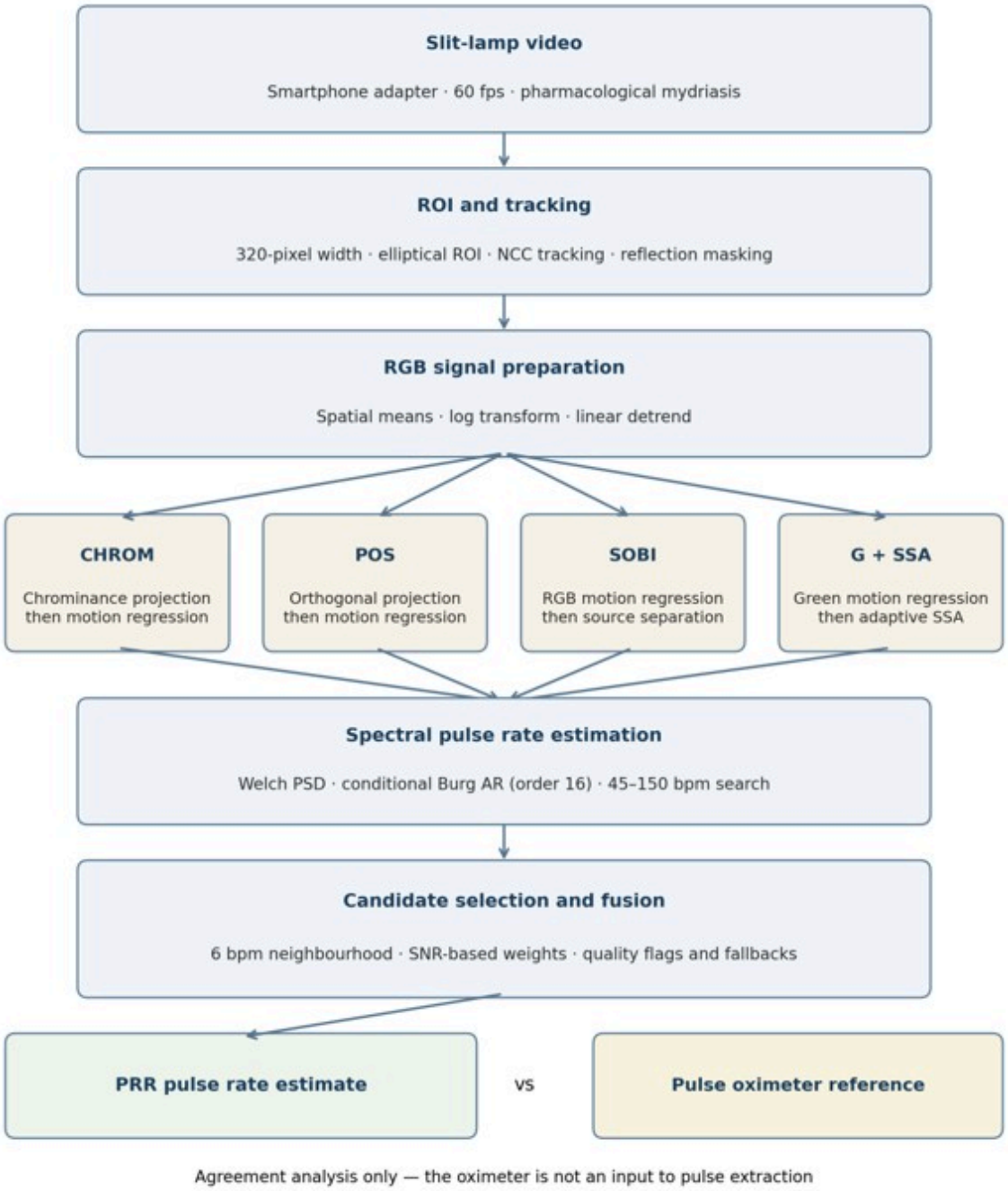


Figure 2

PRR Analyzer v47 processing overview